

## Thermal decomposition behavior of the HfO<sub>2</sub>/SiO<sub>2</sub>/Si system

S. Sayan and E. Garfunkel<sup>a)</sup>

*Department of Chemistry, Rutgers University, Piscataway, New Jersey 08854*

T. Nishimura, W. H. Schulte, and T. Gustafsson

*Department of Physics and Astronomy, Rutgers University, Piscataway, New Jersey 08854*

G. D. Wilk

*Electronic Device Research Laboratory, Agere Systems, Murray Hill, New Jersey 07974*

(Received 27 January 2003; accepted 9 April 2003)

We report on the thermal decomposition of uncapped, ultrathin HfO<sub>2</sub> films grown by chemical vapor deposition on SiO<sub>2</sub>/Si(100) substrates. Medium energy ion scattering, x-ray photoelectron spectroscopy, scanning electron microscopy and atomic force microscopy were used to examine the films after they had been annealed in vacuum to 900–1050 °C. Film decomposition is a strong function of the HfO<sub>2</sub> overlayer thickness at a given temperature, but the underlying SiO<sub>2</sub> layer thickness does not significantly affect the thermal stability of the HfO<sub>2</sub> film. Oxygen diffusion in the system was monitored by <sup>16</sup>O/<sup>18</sup>O isotopic labeling methods. Direct evidence of silicide formation is observed upon decomposition. © 2003 American Institute of Physics.

[DOI: 10.1063/1.1578525]

### INTRODUCTION

The limit for conventional metal–oxide–semiconductor field-effect-transistor (MOSFET) gate dielectric scaling is rapidly approaching due to gate leakage. More specifically, the use of SiO<sub>2</sub> and SiO<sub>x</sub>N<sub>y</sub> dielectric layers below 1.2 nm will result in unacceptable gate leakage currents for many applications. Continued scaling will soon require a ~1 nm equivalent gate oxide thickness.<sup>1</sup> One solution being extensively explored is to increase the gate capacitance by replacing SiO<sub>x</sub>N<sub>y</sub> with higher permittivity dielectrics. For a given capacitance density (i.e., electrical thickness) any high-*k* dielectric candidate must exhibit lower leakage than SiO<sub>2</sub>.

A large number of alternative gate dielectric materials have been examined during the past few years, including metal oxides such as Ta<sub>2</sub>O<sub>5</sub>, TiO<sub>2</sub>, HfO<sub>2</sub>, ZrO<sub>2</sub>, Y<sub>2</sub>O<sub>3</sub>, Al<sub>2</sub>O<sub>3</sub>, and La<sub>2</sub>O<sub>3</sub>, as well as their silicates and aluminates. Many potential high-*k* materials are not stable on silicon under the processing conditions required, and react at high temperature under equilibrium conditions.<sup>2</sup> Such materials may be isolated from the silicon by using interfacial reaction barrier layers. Barrier layers are often lower-*k* materials, thus limiting the ultimate gate capacitance. A better approach is to avoid the barrier layer by finding a material and processing methodology that is stable to 1000–1100 °C. Considerable attention has been given to HfO<sub>2</sub> due to its relatively high resistivity and dielectric constant (*k*~20). Furthermore, HfO<sub>2</sub> appears to be thermally stable next to silicon at temperatures of up to 1000 °C.<sup>3,4</sup> Recent reports have demonstrated that HfO<sub>2</sub> is indeed stable next to Si with an intentionally grown ultrathin oxide interfacial layer.<sup>5,6</sup>

Unfortunately it has proven extremely difficult to find any high-*k* dielectric material that provides as perfect an interface with silicon as is found with SiO<sub>2</sub>. Interface quality

is crucial since it strongly affects device performance through channel mobility and threshold voltage stability. An optimal gate stack may have 1–2 monolayers of SiO<sub>x</sub>N<sub>y</sub> at the channel interface followed by a high-*k* oxide (or multi-component) film of 1–3nm physical thickness.

The purpose of this article is to develop a better understanding of the thermal stability and decomposition of high-*k* oxides on silicon under high-temperature reducing conditions. Such conditions might arise in a postgrowth anneal when the local O<sub>2</sub> and H<sub>2</sub>O partial pressures are low. In this contribution, we report on the decomposition mechanism and kinetics for HfO<sub>2</sub>/SiO<sub>2</sub>/Si stacks under vacuum annealing conditions.

The thermal decomposition behavior of SiO<sub>2</sub>/Si films has been the subject of many studies, and the decomposition structure, chemistry, and kinetics are now reasonably well understood. High-temperature SiO<sub>2</sub> decomposition from thin films of SiO<sub>2</sub> on Si was studied by Tromp *et al.*<sup>7</sup> using ion scattering and electron microscopy. It was concluded that the SiO<sub>2</sub> initially decomposes at the interface, where a less stable suboxide (SiO<sub>x</sub>) is present, followed by the formation and lateral growth of voids in the oxide. This mechanism thereby exposes regions of atomically clean Si while surrounding oxide areas retain their thickness (i.e., where voids did not form at the interface). The desorbing species is SiO, presumably formed at the Si/SiO<sub>2</sub> interface.

The thermal stability of high-*k* oxides on Si has been reported to be similar to the SiO<sub>2</sub>/Si case.<sup>8–10</sup> Jeon *et al.* studied the chemical stability of ultrathin ZrO<sub>2</sub> films grown by chemical vapor deposition as a function of thermal treatment in vacuum and N<sub>2</sub> ambient.<sup>11</sup> Although the chemical structure was stable up to 800 °C in vacuum, a 900 °C anneal in an ambient devoid of oxygen results in silicide formation.<sup>11</sup> The mechanism proposed was the formation of gaseous SiO species at an interfacial SiO<sub>x</sub> layer at

<sup>a)</sup>Electronic mail: garfunk@rutchem.rutgers.edu

high temperatures, and reaction of these species with  $\text{ZrO}_2$  forming silicides. Chang and Lin examined the thermal stability of  $\text{ZrO}_2/\text{ZrSi}_x\text{O}_y/\text{SiO}_2$  thin films grown by rapid thermal chemical vapor deposition (RT CVD) on silicon by soft x-ray photoemission spectroscopy (SXPS). The films were found to be stable up to  $880^\circ\text{C}$  in vacuum at which point the films decomposed and formed zirconium silicides.<sup>12,13</sup> Reduced oxygen and zirconium photoemission intensities were attributed to the formation and desorption of gaseous  $\text{ZrO}$  and  $\text{SiO}$  species and rationalized by considering the thermodynamics.

Phase identification and epitaxial structure of the silicides have also been studied by others. Zaima *et al.* showed that annealing e-beam evaporated Hf on Si results in  $\text{Hf}_2\text{Si}_3$ ,  $\text{HfSi}$ , and eventually  $\text{HfSi}_2$  phases appearing with increased temperature, in agreement with previous work on phase determination.<sup>13</sup> The epitaxial relationship was found to be  $(110)\text{Hf}_2\text{Si}_3//\text{Si}(100)$  and  $[001]\text{Hf}_2\text{Si}_3//[110]\text{Si}$ , with a lattice mismatch of about 4.4% and 29%, respectively. Chang *et al.* showed that when Hf/Si samples are annealed to  $1100^\circ\text{C}$ , islands of  $\text{HfSi}_2$   $0.8\ \mu\text{m}$  in average grain size cover about 40% of the surface.<sup>14</sup> The crystallographic relationships between  $\text{HfSi}_2$  and the  $\text{Si}(100)$  substrate were reported to be  $[010]\text{HfSi}_2//[001]\text{Si}$  and  $(002)\text{HfSi}_2//(220)\text{Si}$  with about a 1% lattice mismatch.

## EXPERIMENTAL PROCEDURE

We have used medium-energy ion scattering (MEIS),<sup>15</sup> a high-resolution, lower energy ( $\sim 100\ \text{keV}$ ) version of Rutherford backscattering spectroscopy (RBS), to obtain compositional depth profiles of ultrathin gate dielectrics. The use of a high resolving power electrostatic ion energy analyzer gives a depth resolution much better than that of RBS.<sup>16</sup> The areal densities of the different elements were extracted from the MEIS spectra, and the depth profiles of the elements were obtained from simulations of the ion energy distributions using the known film density and energy loss. In cases where the density of films is not known, reasonable approximations were used.<sup>17</sup> Quantitative depth profiles for different species are extracted with resolution as high as  $3\ \text{\AA}$  at the surface. Due to the statistical nature of the ion–solid interaction, the depth resolution deteriorates for deeper layers (ion straggling). Although for  $\text{HfO}_2$  films the calculated absolute depth resolution is  $\sim 8\ \text{\AA}$  at a depth of  $30\ \text{\AA}$ , relative changes in film (or interface layer) thickness at  $30\ \text{\AA}$  are known to better than  $2\ \text{\AA}$ . The beam size in our MEIS setup is of the order of  $\sim 0.1\ \text{mm}^2$ , therefore the data represent averages over this sampling area. It should be noted that this fact makes it difficult to distinguish between near-interface compositional gradients and interface or surface roughness.

Our MEIS measurements are performed using a channeling and blocking configuration. In this geometry, the incident and scattered ion beams are aligned along a crystallographic axis of the substrate. This reduces the background scattering from the substrate significantly and therefore increases the sensitivity to the overlayer material. The inset in Fig. 1 demonstrates the configuration used in these measurements. The incident  $97.8\ \text{keV}\ \text{H}^+$  ion is aligned along the  $\langle 100 \rangle$  direc-

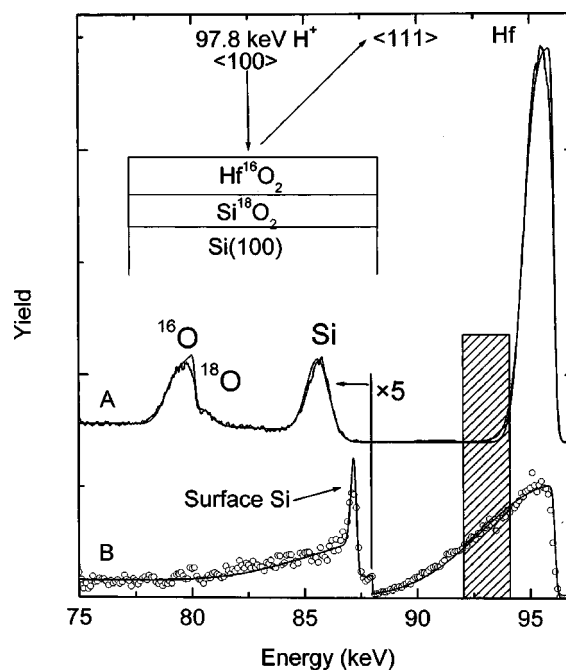


FIG. 1. MEIS spectra of the  $26\ \text{\AA}\ \text{HfO}_2/\text{SiO}_2/\text{Si}$  sample (a) as deposited and (b) after decomposition at  $1000^\circ\text{C}$ . The inset demonstrates the measurement configuration.

tion (the surface normal) and the scattered beam is measured in the  $\langle 111 \rangle$  direction.

$\text{Si}(100)$   $p$ -type ( $\rho = 1 - 5\ \Omega\ \text{cm}$ ) substrates were used in all studies. Hydrogen-terminated  $\text{Si}(100)$  substrates were prepared by wet chemical methods using the following procedure: (i) the wafers were rinsed in high purity water and dipped in a solution of  $\text{HCl}:\text{H}_2\text{O}_2:\text{H}_2\text{O}$  (2:1:1) at  $70^\circ\text{C}$  for 10 min, (ii) the wafers were then rinsed in water and dipped in a dilute solution of  $\text{HF}:\text{H}_2\text{O}$  (1:20) for 10 s and then rinsed in pure water. After repeating the above cycle twice, the sample was immediately introduced into a quartz furnace. First, the clean sample was preoxidized at  $550^\circ\text{C}$  under an  $^{18}\text{O}_2$  pressure of 0.1 Torr for 12 h and then further oxidized at high temperature for various times to form different  $\text{SiO}_2$  thicknesses. The samples discussed here were annealed at 750, 850, and  $900^\circ\text{C}$  under an  $^{18}\text{O}_2$  pressure of  $1 \times 10^{-2}$ , 0.1, and 1 Torr for 30 min, 30 min, and 6 h. After these treatments, the thicknesses of the  $\text{Si}\ ^{18}\text{O}_2$  layers were 10, 17, and  $33\ \text{\AA}$ , as determined by MEIS.  $\text{Hf}^{16}\text{O}_2$  layers with thicknesses ranging from 26 to  $56\ \text{\AA}$  were then deposited by CVD, as described elsewhere.<sup>18</sup> These samples were introduced into the MEIS ultrahigh vacuum chamber, degassed at  $550^\circ\text{C}$  for 12 h, then resistively heated to  $920 - 1000^\circ\text{C}$ . The temperature was monitored using an IR pyrometer (emissivity of  $\sim 0.7$ ). The operating pressure rises to at most  $3 \times 10^{-8}$  Torr during the high temperature annealing. Decomposition of the overlayers was monitored *in situ* using the intensity of the Hf signal in the MEIS spectrum. Well-established methods were used to minimize the proton beam dose to avoid beam damage.

The surface roughness of the CVD-grown films was determined independently by atomic force microscopy and secondary electron microscopy. X-ray photoelectron measure-

TABLE I. Total amount of hafnium in the as-deposited and annealed samples measured in both channeling and  $7^\circ$  off-channel configurations. The absolute errors are 2%–3%.

Sample	Detected Hf atoms ( $\times 10^{15}$ atoms/cm $^2$ )	
	$\langle 001 \rangle$ direction	Random direction
As deposited	8.0	7.8
Annealed at 1000 °C	6.6	8.1

ments were performed in a Kratos XSAM 800 spectrometer using Mg  $K\alpha$  excitation ( $h\nu = 1253.6$  eV). The binding energies (BEs) reported are referenced to the Au  $4f_{7/2}$  photoelectron line (BE = 84.0 eV). The carbon contamination in the films was mostly located at the surface; bulk carbon levels were below the limit of MEIS sensitivity for carbon.

## RESULTS AND DISCUSSION

Figure 1(a) shows a backscattered proton energy spectrum of the as-deposited HfO $_2$  film on a 26 Å thermal Si $^{18}$ O $_2$ /Si film. The total amounts of Hf,  $^{16}$ O, and  $^{18}$ O in the film were determined to be  $7.1 \times 10^{15}$ ,  $1.5 \times 10^{16}$ , and  $3.4 \times 10^{15}$  atoms/cm $^2$ , respectively. The position of the Si peak indicates that no Si is located at the outer surface (which might have resulted from nonuniform growth, outdiffusion, etc). When using the known relative backscattering cross sections, the simulation yields a slightly O-rich HfO $_{2.17 \pm 0.06}$  film with a thickness of about 26 Å.

In several sets of experiments, we determined the time necessary to decompose the film at fixed temperature. Determination of the decomposition time was accomplished through the following MEIS-based method. We monitor the Hf ion scattering yield at depth larger than that corresponding to the thickness of the HfO $_2$  film. An increase in the signal strength at an energy just below that where it is observed for the as-deposited film occurs only at very high temperature when Hf diffuses into the substrate. In other words, decomposition of HfO $_2$  was monitored via an increase in the ion scattering intensity in the vicinity of the low energy edge of the Hf MEIS signal [e.g., the shaded area in Fig. 1(b)]. For the purposes of this article, we say the film has decomposed when we observe a 10% increase in the low-energy edge of Hf signal relative to that of the Hf peak signal.

Annealing the as-deposited films [e.g., those shown in Fig. 1(a)] to 1000 °C in vacuum results in clear changes in the spectrum as a function of time; see Fig. 1(b). Eventually the oxygen signal disappears. The position of the silicon peak indicates that Si is now present on the surface, and the hafnium diffuses deeper into the substrate ( $\sim 160$  Å).

The total amounts of hafnium present in a 29 Å HfO $_2$  as-deposited sample before and after decomposition are given in Table I. When monitored in standard channeling and blocking alignment, it seems as though  $\sim 18\%$  of the total hafnium is lost during this initial annealing process. The MEIS Hf signal increases, however, when we align the incident and exit angles to a  $\sim 7^\circ$  off-channel direction. In the latter geometry, the ion beam samples all atoms in the film, while in channeling geometry, if the atoms are arranged in a

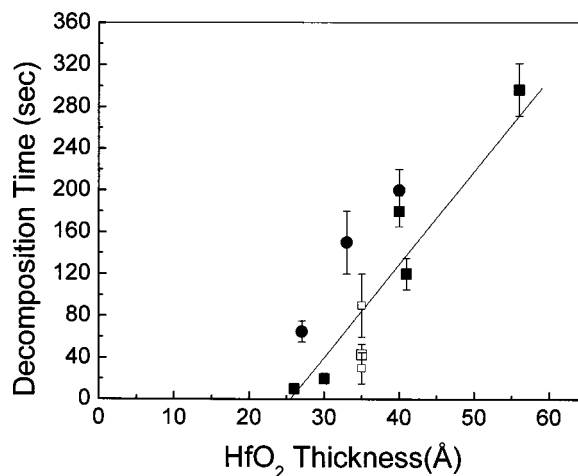


FIG. 2. Decomposition time vs the HfO $_2$  film thickness measured at 1000 °C. ■ CVD HfO $_2$  on 9 Å thermal Si $^{18}$ O $_2$ /Si, ● CVD HfO $_2$  on 11 Å thermal Si $^{18}$ O $_2$ /Si, and □ ALCVD HfO $_2$  on 8 Å SiO $_2$ /Si.

regular array, some subsurface atoms will not be detected. The amount observed after annealing in this “random” geometry is the same as in the as-deposited case (within 2%), hence it may safely be stated that there is no measurable loss of hafnium upon decomposition. This result indicates that HfSi $_x$  crystallites are likely formed and preferentially oriented in the  $\langle 001 \rangle$  direction.

In order to study the effect of HfO $_2$  film thickness on the decomposition time, a series of samples with different thicknesses were prepared. Figure 2 indicates that the decomposition time is strongly dependent on the HfO $_2$  film thickness. There appears to be an approximately linear relationship between the HfO $_2$  overlayer thickness and decomposition time over the small range of conditions studied. The plot implies that films less than  $\sim 26$  Å will decompose quickly at 1000 °C in vacuum. In the same plot, the data for ALD-grown HfO $_2$  films are also included (open squares). There is very good agreement with the CVD data. This suggests that the decomposition process is a material property of the HfO $_2$  and does not depend on the nature of these growth processes.

The temperature dependence of the decomposition time for a given film thickness was also investigated, and reveals simple Arrhenius behavior with an effective activation energy of 437 kJ/mole (4.5 eV), as shown in Fig. 3. This activation energy (for the initial decomposition of HfO $_2$  thin films on thermal oxides) is somewhat higher than that determined by Smith and Ghidini for the growth and decomposition of ultrathin SiO $_2$  under reduced pressure via SiO desorption (3.83 eV).<sup>19</sup> On the other hand, the activation energy for void growth in pure SiO $_2$ /Si decomposition was found to be about  $\sim 2$  eV by Liehr *et al.*<sup>20</sup> The fact that the value obtained here is appreciably higher than the reported values for SiO desorption and void growth suggests that SiO diffusion/desorption through the gate stack may be the rate-determining step in initiating the decomposition process for this HfO $_2$ /SiO $_2$ /Si gate stack, and is consistent with the observation of a thickness dependence for HfO $_2$  but not for SiO $_2$ .

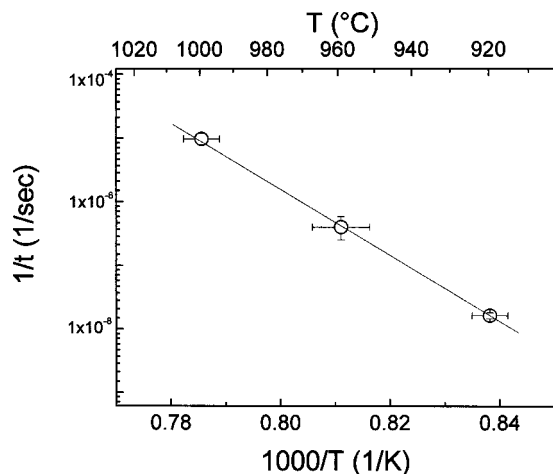


FIG. 3. Arrhenius plot of the temperature dependence of the decomposition time for a  $\sim 26 \text{ \AA}$   $\text{HfO}_2/\text{Si}^{18}\text{O}_2/\text{Si}$  film.

The thickness of the bottom oxide was also varied in order to observe the effects of this layer on film decomposition. A plot of  $\text{SiO}_2$  thickness versus decomposition time is given in Fig. 4. Somewhat surprisingly, the dependence on the  $\text{SiO}_2$  layer thickness appears quite insignificant within the range of 10–33 Å used in this study.

In an attempt to assess the diffusion that occurs prior and during thermal decomposition of the  $\text{HfO}_2$  films, one of the isotopically prepared samples was annealed at 1000 °C for 10 s (Table II). The changes in film composition were measured by MEIS. The isotopically labeled oxygen ( $^{18}\text{O}$ ) in the interfacial oxide layer provides evidence of the migration/diffusion of these species upon heating. The MEIS spectra of the sample before and after anneal are shown in Fig. 5. In Fig. 6, the composition profile obtained after a simulation of the backscattered ion energy distribution is given. The spectra obtained before and after annealing reveal that the high-energy edge of  $^{18}\text{O}$  shifts toward higher backscattered ion energies, indicating that this species from the bottom oxide diffuses toward the surface, producing a much more uniform  $^{18}\text{O}$  distribution throughout the film. Meanwhile, the low-energy edge of  $^{16}\text{O}$  tails toward lower energies indicating that this species diffuses into the bottom ox-

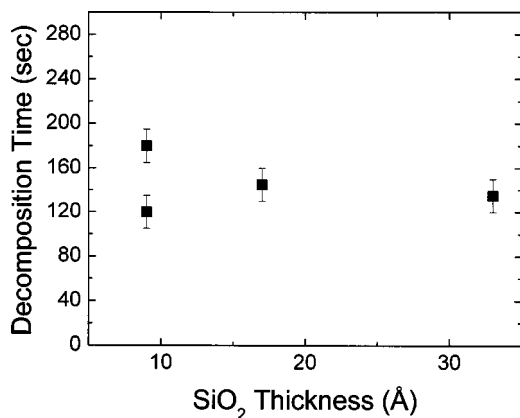


FIG. 4. Plot of the  $\text{SiO}_2$  interfacial thickness vs the decomposition time. The  $\text{HfO}_2$  overlayer films thickness is 37 Å.

TABLE II. Total amounts of Hf,  $^{18}\text{O}$ , and  $^{16}\text{O}$  in a 26 Å  $\text{HfO}_2/\text{SiO}_2/\text{Si}$  system before and after a 10 s anneal at 1000 °C

Sample	Hf	Si	$^{18}\text{O}$	$^{16}\text{O}$
Substrate		6.5	3.4	0.8
26 Å $\text{HfO}_2$ as is	7.1	6.6	3.4	15.4
			18.8	
Annealed at 1000 °C, 10 s	7.3	6.0	2.5	14.2
			16.7	

ide. The inset shows the difference spectrum, which exhibits a positive and a negative feature. The integrated area under the negative feature is more than that of the positive feature, however, which indicates loss of oxygen from the gate stack. Although deconvolution of the oxygen region is nontrivial due to the overlap in  $^{16}\text{O}$  and  $^{18}\text{O}$  peaks, the total oxygen amount decreases *prior* to decomposition of the  $\text{HfO}_2$  film. It is also worth noting the shrinkage of the total visible silicon MEIS peak width.

There are many hypotheses that can be (and in some cases have been) proposed to explain the initial decomposition. We summarize several of these in Fig. 7. Key in all is to remember that Hf and Zr have a higher oxygen affinity than Si, thus  $\text{SiO}_2$  should in principle disappear before  $\text{HfO}_2$  or  $\text{ZrO}_2$ . In one model,  $\text{SiO}$  forms at the internal interface at high temperature, where it builds up pressure (and forms an internal bubble) [Fig. 7(a)]. When it exceeds a certain critical pressure locally or finds appropriate defects, it would evolve from the surface and form pinholes [Fig. 7(d)]. Subsequently, both  $\text{HfO}_2$  and  $\text{SiO}_2$  would react with Si and liberate more  $\text{SiO}$ . The voids (devoid of metal and silicon oxide) should expand across the surface [Fig. 7(e)], leaving metal silicide to crystallize in the most Si rich phase available (since it is in excess). Another model has O atoms outdiffusing through the film and desorbing at the surface, following surface recombination to form molecules (e.g.,  $\text{SiO}$  or  $\text{O}_2$ ). We and others have observed  $\text{SiO}$  desorption, although it is not clear if there is some  $\text{O}_2$  or  $\text{H}_2\text{O}$  desorption during the initial stages<sup>21</sup> [Fig. 7(c)], or if Si can itself outdiffuse and react with O at the

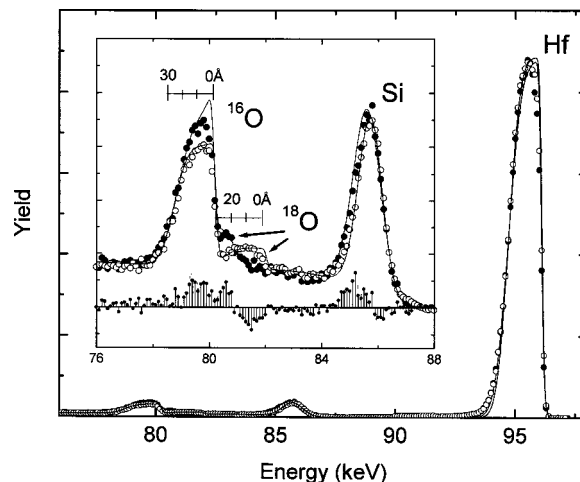


FIG. 5. MEIS spectra of 26 Å  $\text{HfO}_2/9 \text{ \AA}$   $\text{Si}^{18}\text{O}_2/\text{Si}$ . Inset: Closeup of the 76–88 keV region. • As-deposited sample and ○ same sample annealed at 1000 °C for 10 s.

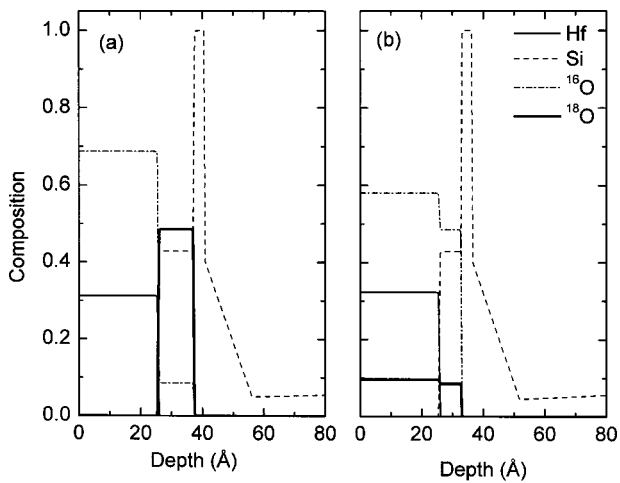


FIG. 6. Compositional profile obtained after simulation of the backscattered ion energy distribution for 26 Å HfO<sub>2</sub>/9 Å Si<sup>18</sup>O<sub>2</sub>/Si (a) as deposited and (b) after 10 s annealing at 1000 °C.

surface and form SiO [Fig. 7(b)]. The latter case is more probable with Y, La, Gd, or other metal oxides that readily form silicates.<sup>8</sup> In all cases, we believe that voids eventually form, analogous to in the SiO<sub>2</sub>/Si system. These voids then

spread across the entire surface and leave metal silicide islands. If the desorbing O is supplied by the buried SiO<sub>2</sub> layer, then that layer may become thin prior to HfO<sub>2</sub> decomposition. Some of our results imply this does happen, however it may be occurring in parallel with O being supplied from (the slightly oxygen-rich) HfO<sub>2</sub> layer. On the other hand, eventually the HfO<sub>2</sub> itself must react with Si and form hafnium silicide, with O desorbing into the gas again as SiO.

Our results indicate that the oxygen partial pressure is critical in defining when the film decomposes.<sup>6</sup> Rapid thermal anneal (RTA) studies of ZrO<sub>2</sub>/Si done in N<sub>2</sub>, on the other hand, did not show evidence of decomposition of the films.<sup>11</sup> Two possible explanations were put forward for the observed result, one being the reaction of the interfacial layer (SiO<sub>x</sub> formed during deposition) with the substrate forming SiO(g), and the other was the presence of a small amount of O<sub>2</sub> in the N<sub>2</sub> gas, which suppresses the reducing effect of the N<sub>2</sub> atmosphere.

Related to this is the behavior of a high-*k* stack with a poly-Si cap. In this case, the silicon cap also provides a reducing environment during the anneals (O cannot enter the system because Si provides an effective diffusion barrier, presumably even in oxidizing anneals), and silicide forma-

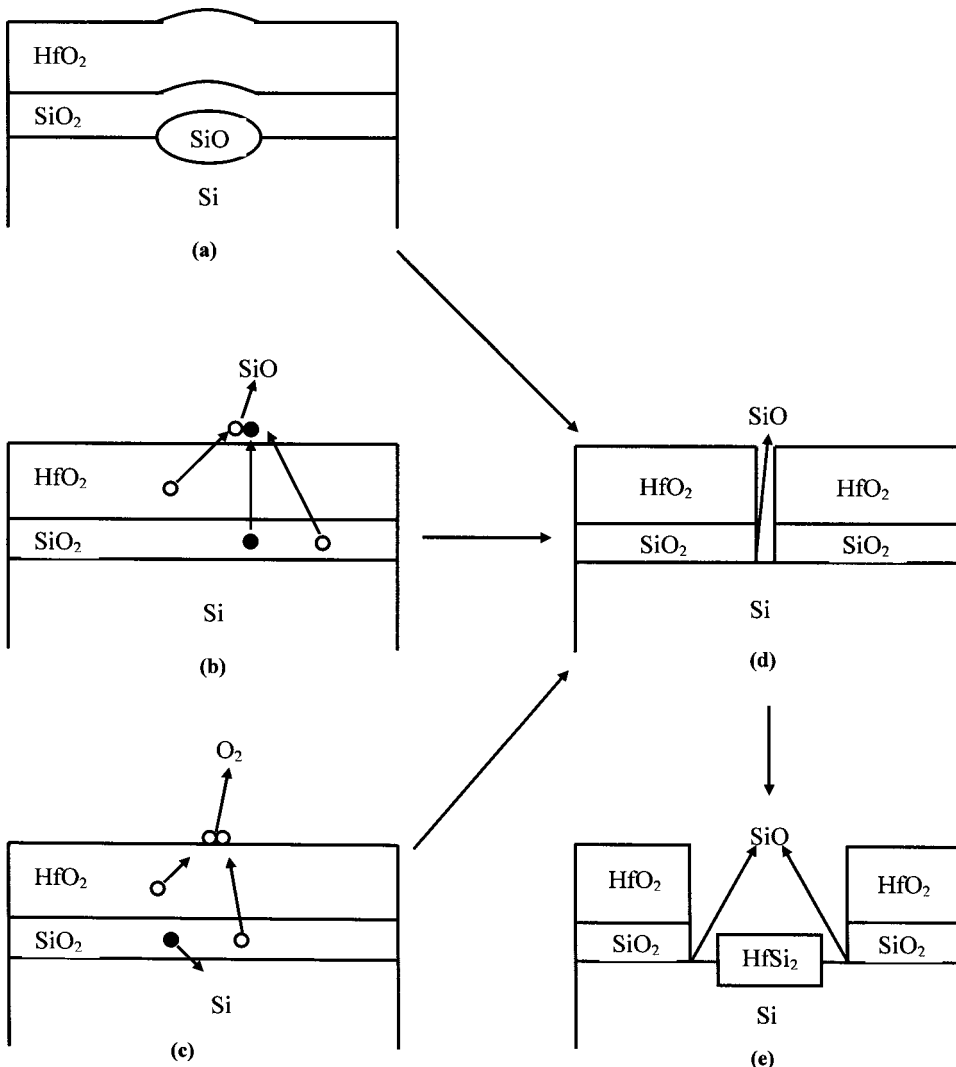


FIG. 7. Four possible decomposition initiation schemes (a) – (d) and eventual fate of annealed HfO<sub>2</sub>/SiO<sub>2</sub>/Si structures: (a) internal SiO pressure buildup, (b) Si and O outdiffusion/surface recombination/SiO desorption, (c) O outdiffusion/O<sub>2</sub> formation/desorption/Si recrystallization, (d) pinhole formation, and (e) void growth/silicide crystallization.

tion is sometimes observed. What is less obvious is where the O goes during the anneal, as, in principle, it cannot escape as SiO(g). In one argument, the oxide becomes slightly reduced during poly-Si deposition, which then reacts with overlayer silicon, leaving a metal silicide and a stoichiometric metal oxide. Other arguments are that entropy drives some metal into the silicon and/or that the system is not in equilibrium.

Although we cannot yet argue definitively which is the dominant initial step, we clearly see that SiO is desorbed, and that the oxide overlayer decomposes by forming ever larger voids on the surface and leaves silicide islands. Although we did not determine the stoichiometry of the hafnium silicide formed in this study, in light of the studies of Chang *et al.*<sup>14</sup> and of Zaima *et al.*,<sup>13</sup> at this high temperature, Si-rich silicides such as HfSi<sub>2</sub> are likely to have formed due to the essentially unlimited supply of silicon from the substrate (facilitating formation of the most silicon-rich silicide). The preferential formation of crystallites on Si(100) (lattice mismatch of ~1%), which we showed above by off-channeling MEIS measurements, further supports the hypothesis of HfSi<sub>2</sub> crystallites after decomposition.

Another important aspect of the extent of hafnium diffusion into the substrate that forms hafnium silicide is that the hafnium diffuses as much as 160 Å into the substrate after decomposition. Any surface analysis with only shallow (several nm) depth information will show this as a loss of metal. We believe, in light of our MEIS results and our understanding of the phase behavior, that Zr and Hf do not desorb.

In an attempt to observe morphological changes on the surface of the HfO<sub>2</sub> films under investigation, a 26 Å HfO<sub>2</sub>/SiO<sub>2</sub>/Si sample was intentionally resistively heated unevenly in order to produce a temperature gradient across the wafer. This resulted in a temperature gradient of about 40 °C (930–970 °C) across the sample. The low and high temperature parts of the sample are referred to as “zone L” and “zone H,” respectively, below.

After *in situ* MEIS measurement, the sample was analyzed by *ex situ* XPS. XPS studies help determine the change in chemical state of this film after decomposition. The XPS system has a sampling area ~4 × 4 mm. The spectra obtained from various regions across the sample are shown in Fig. 8. The spectrum for the as-deposited sample is shown for comparison. The Hf 4*f* spin-orbit doublet has splitting of ~1.55 eV and the binding energy of Hf 4*f*<sub>7/2</sub> of HfO<sub>2</sub> was found to be located at 17.7 eV. Spectra obtained from the H zone have an additional spin-orbit doublet located at 14.9 eV which is consistent with a silicide species.

On the same sample, scanning electron microscopy (SEM) was performed to observe surface features (Fig. 9) of this sample. The low and high temperature zones are indicated. At some transition region “zone T”, voids of various size are observed (20–50 μm). It is worth noting that the density of voids is higher towards the low temperature zone whereas the void size increases towards the high temperature zone, suggesting the coalescence of smaller voids forms larger ones. This micrograph also shows that the decomposition occurs rapidly at a well-defined temperature.

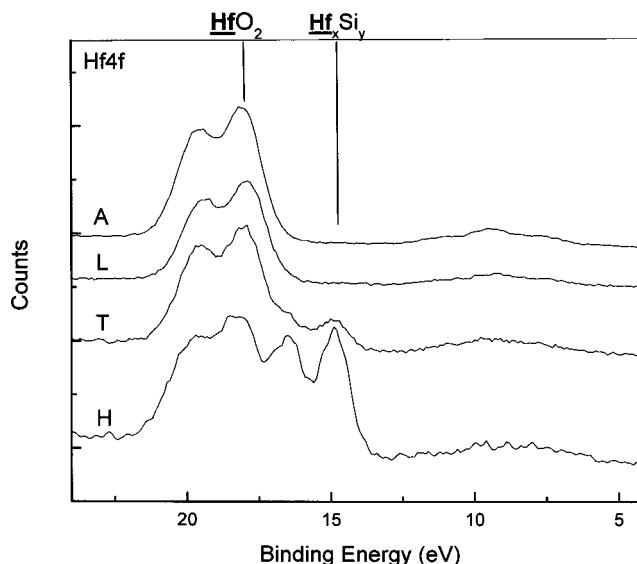


FIG. 8. XPS spectra of Hf 4*f* from three different temperature zones across a partially decomposed sample. (L) Low-temperature zone, (T) transition zone, and (H) high-temperature zone.

## CONCLUSIONS

The decomposition behavior of a HfO<sub>2</sub>/SiO<sub>2</sub>/Si gate stack in a reducing environment was investigated. We believe that vacuum anneals can serve as a useful model for annealing studies of gate stacks. The decomposition time is strongly dependent on the HfO<sub>2</sub> film thickness, but appears nearly independent of the SiO<sub>2</sub> bottom layer thicknesses used in this study. The decomposition process is a material property of the metal oxide and does not depend on the nature of the growth process. The temperature dependence of the decomposition time shows simple Arrhenius behavior with an effective activation energy of ~4.5 eV.

Several models were discussed to explain the decomposition. Regardless of the initial step, voids open up and spread rapidly across the surface at a well-defined temperature. Complete decomposition results in silicide formation and the disappearance of oxygen.

Our results support a picture where the film reaction processes occur in the following sequence as a function of the

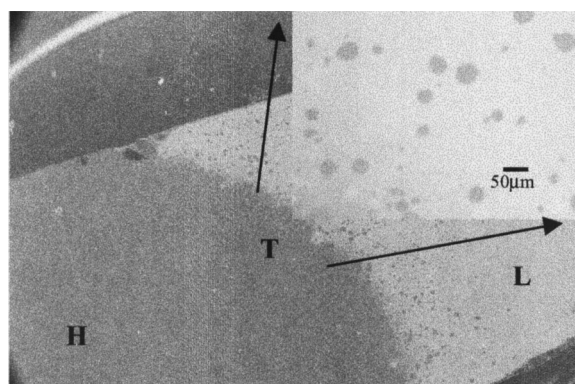
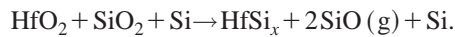


FIG. 9. SEM micrograph showing the high- (H) and low- (L) temperature sides of the sample along with the transition (T) region. Scale mark of the inset corresponds to 50 μm (×13 of large area micrograph).

anneal temperature (and time): oxygen exchange between the HfO<sub>2</sub> and the SiO<sub>2</sub>, HfO<sub>2</sub> crystallization, SiO desorption, Hf indiffusion, and silicide formation where the HfSi<sub>x</sub> crystal-lites are preferentially oriented in the ⟨001⟩ direction.

The overall process can be written as



## ACKNOWLEDGMENTS

The authors would like to acknowledge the support of the Semiconductor Research Corporation. They also note helpful suggestions from S. Stemmer, J. P. Maria, E. Gusev, M. Copel, P. McIntyre, and D. Starodub during various parts of this work.

<sup>1</sup>ITRS, 2002 ed. (Semiconductor Industry Association, San Jose, CA, 2000), <http://public.itrs.net/>

<sup>2</sup>K. J. Hubbard and D. G. Schlom, *J. Mater. Res.* **11**, 2757 (1996).

<sup>3</sup>I. Barin and O. Knacke, *Thermodynamic Properties of Elements and Oxides* (Springer, Berlin, 1973).

<sup>4</sup>S. J. Lee, H. F. Luan, W. P. Bai, C. H. Lee, T. S. Jeon, Y. Senzaki, D. Roberts, and D. L. Kwong, High Quality Ultrathin CVD HfO<sub>2</sub> Gate Stack with Poly-Si Gate Electrode, San Francisco, CA, 2000, pp. 2.4.1 – 2.4.4.

<sup>5</sup>C. Hobbs *et al.*, 80 nm Poly-Si Gate CMOS with HfO<sub>2</sub> Gate Dielectric, Washington, DC, IEDM 2001, pp. 30.1.1 – 30.1.4.

<sup>6</sup>E. P. Gusev *et al.*, Ultrathin High-*K* Gate Stacks for Advanced CMOS Devices, Washington, DC, IEDM 2001, pp. 20.1.1 – 20.1.4.

<sup>7</sup>R. Tromp, G. W. Rubloff, P. Balk, F. K. LeGoues, and E. J. van Loenen, *Phys. Rev. Lett.* **55**, 2332 (1985).

<sup>8</sup>M. Copel, personal communication (2002).

<sup>9</sup>J.-P. Maria, D. Wicaksana, A. I. Kingon, B. Busch, W. H. Schulte, E. Garfunkel, and T. Gustafsson, *Appl. Phys. Lett.* **90**, 3476 (2001).

<sup>10</sup>S. Stemmer, C. Zhiqiang, R. Keding, J.-P. Maria, D. Wicaksana, and A. Kingon, *J. Appl. Phys.* **92**, 82 (2002).

<sup>11</sup>T. S. Jeon, J. M. White, and D. L. Kwong, *Appl. Phys. Lett.* **78**, 368 (2001).

<sup>12</sup>J. P. Chang and Y.-S. Lin, *Appl. Phys. Lett.* **79**, 3824 (2001).

<sup>13</sup>S. Zaima, N. Wakai, T. Yamauchi, and Y. Yasuda, *J. Appl. Phys.* **74**, 6703 (1993).

<sup>14</sup>C. S. Chang, C. W. Nieh, and L. J. Chen, *J. Appl. Phys.* **61**, 2393 (1987).

<sup>15</sup>J. F. van der Veen, *Surf. Sci. Rep.* **5**, 199 (1985).

<sup>16</sup>R. M. Tromp, M. Copel, M. C. Reuter, M. H. v. Hoegen, J. Speidell, and R. Koudijs, *Rev. Sci. Instrum.* **62**, 2679 (1991).

<sup>17</sup>E. P. Gusev, H. C. Lu, T. Gustafsson, and E. Garfunkel, *Phys. Rev. B* **52**, 1759 (1995).

<sup>18</sup>S. Sayan, S. Aravamudhan, B. W. Busch, W. H. Schulte, F. Cosandey, G. D. Wilk, T. Gustafsson, and E. Garfunkel, *J. Vac. Sci. Technol. A* **20**, 507 (2002).

<sup>19</sup>F. W. Smith and G. Ghidini, *J. Electrochem. Soc.* **129**, 1300 (1982).

<sup>20</sup>M. Liehr, J. E. Lewis, and G. W. Rubloff, *J. Vac. Sci. Technol. A* **5**, 1559 (1987).

<sup>21</sup>C. M. Perkins, B. B. Triplett, P. C. McIntyre, K. C. Saraswat, and E. Shero, *Appl. Phys. Lett.* **81**, 1417 (2002).